Front. Biol. China 2007, 2(1): 75–79
DOI 10.1007/s11515-007-0013-7

RESEARCH ARTICLE

# Effects of Arg26 and Lys27 mutation on the bioactivity of HNTX-IV

**XIONG Xia, XU Xia, LI Dongling, CHEN Ping, LIANG Songping (✉)**

College of Life Sciences, Hunan Normal University, Changsha 410081, China



**Abstract** Hainantoxin-IV (HNTX-IV) was isolated from the Chinese bird spider *Ornithoctorcs hainana* and identified as a novel antagonist of tetrodotoxin-sensitive (TTX-S) sodium channels. As revealed by the solution structure of HNTX-IV solved by two-dimensional nuclear magnetic resonance (2D-NMR), HNTX-IV adopts an inhibitor cystine knot motif. To check the role of basic residues during HNTX-IV's interaction with TTX-S sodium channels, R26A and K27A mutants of HNTX-IV were constructed by solid-phase chemical synthesis. The synthesized peptides were purified and refolded under optimized oxidation conditions. Correct synthesis and folding were confirmed by MALDI-TOF mass spectrometry and NMR spectroscopy, respectively. Using the whole-cell patch-clamp technique, Lys27 but not Arg26 was identified as a key residue for HNTX-IV's bioactivity against TTX-S sodium channels, because R26A-HNTX-IV showed slightly reduced activity and K27A-HNTX-IV showed almost no inhibition.

**Keywords** Hainantoxin-IV, mutant, solid-phase synthesis, bioactivity

## 1 Introduction

Hainantoxin-IV (HNTX-IV) is a peptide neurotoxin (Liang et al., 1999) purified from the venom of the recently classified spider *Ornithoctorcs hainana* found in south China. HNTX-IV is composed of 35 amino acid residues with a molecular weight of 3 988.58 Da, and its sequence was identified as: $NH_2$-ECLGFGKGCNPSNDQCCKSSNLVCSRKHRWCKYEI-$CONH_2$.

Electrophysiological investigation of HNTX-IV on rat dorsal root ganglion (DRG) neurons showed that HNTX-IV had a dose-dependent inhibition of tetrodotoxin-sensitive (TTX-S) sodium currents with an $IC_{50}$ value of 34.0 nM. But the activation and inactivation kinetics of sodium currents were not affected by HNTX-IV, which proved that HNTX-IV is most likely a site 1 toxin against sodium channels (Peng et al, 2002; Liu et al., 2003).

As shown by the solution structure of HNTX-IV solved by $^1$H two-dimensional nuclear magnetic resonance (2D-NMR), HNTX-IV adopts a typical ICK motif that has been identified in numerous inhibitors from a variety of life-forms. Structural comparison and sequence alignment of HNTX-IV with other inhibitor cystine knot motif (ICK) toxins revealed that the residues R26 and K27 in the loop IV of HNTX-IV might be involved in its interaction with TTX-S sodium channels. To confirm this hypothesis, R26A-HNTX-IV and K27A-HNTX-IV mutants were obtained by solid-phase chemical synthesis using Fmoc chemistry on a Pioneer Peptide Synthesizer System, followed by optimized oxidation-refolding procedures. Activities of the R26A and K27A mutants against TTX-S sodium channels were assayed and the differentiated roles of Arg26 and Lys27 in HWNX-IV's bioactivity were compared.

## 2 Materials and methods

### 2.1 Materials

Fmoc-PAL-PEG-PS resin was purchased from Applied Biosystems and Fmoc-protected amino acids from Chemassist Corp. Dimethylformamide, piperidine, GSSG, GSH, peptide coupling reagents TBTU and HOBt, trifluoroacetic acid (TFA), α-cyano-4-hydroxy cinnamic acid (CCA), ethanedithiol and thioanisole were obtained from Sigma-Aldrich Corp. All other reagents used were analytical grade.

Translated from *Chinese Journal of Biochemistry and Molecular Biology*, 2005, 21(4): 499−503 [译自: 中国生物化学与分子生物学报]

E-mail: liangsp@hunnu.edu.cn

## 2.2 Methods

### 2.2.1 Mutant synthesis

The general synthetic protocols were performed as described previously by Dai and Liang (2003) and Xiao and Liang (2003). The first Fmoc-amino acid Ile in the C-terminal was coupled twice manually and the other Fmoc-amino acids were synthesized on an automatic peptide synthesizer. Mutant synthesis was accomplished on a 0.1-mmol scale using five-fold excess of Fmoc-amino acid. After the completion of the chain assembly, cleavage of the synthesized peptide from the resin and side-chain deprotection were simultaneously achieved by treating with reagent K (82.5% TFA, 5% double distilled $H_2O$, 5% phenol, 5% thioanisole, and 2.5% ethanedithiol) at 25°C for 2.5 h. The crude synthetic products were fractionated on a semi- preparative reversed- phase C18 column (Vydac C18, 10 mm × 250 mm) mounted to a Waters HPLC Workstation (solvent A, 0.1% aqueous TFA; solvent B, acetonitrile with 0.1% TFA; elution gradient, 15%−45% B over 0−45 min; flow rate, 1 mL/min). The eluted fractions were collected and then analyzed by matrix-assisted laser desorption/ionization time of flight mass spectrometry (MALDI-TOF MS). The peaks of interest were further purified with analytical reversed-phase C18 column (Vydac C18, 4.6 × 250 mm) until a purity of over 95% was achieved.

## 2.3 Oxidation and refolding

Oxidation and refolding of HXNX-IV mutants were conducted as described previously by Wang et al. (2000). Briefly, 0.1 mg of synthesized peptides were loaded to refolding buffer (0.1 mmol/L Tris-HCl, 0.1 mmol/L NaCl, 5 mmol/L GSH, 0.5 mmol/LGSSG at different pH 7.4, 7.8, 8.0, 8.5), and 100 μL samples were taken out at 0 min, 2 min, 5 min, 10 min, 30 min, 1 h, 2 h and 24 h with the addition of 10 μL 50% TFA to stop the reaction. These samples were then analyzed and compared by an analytical reversed-phase C18 column to confirm the optimized conditions.

## 2.4 Identification of the refolded mutants

### 2.4.1 Mass spectrometry

The molecular weights of the crude synthetic products and refolded peptides were checked by MALDI-TOF MS spectrometry (positive mode, 20 kV accelerating voltage and 500 ns delay; 9 μL CCA matrix mixed with 1 μL sample for measurement).

### 2.4.2 NMR spectrometry

NMR samples of native HNTX-IV, R26A-HNTX-IV and K27A-HNTX-IV mutants were prepared by separately dissolving them in 500 μL of 20 mM deuterium sodium acetate buffer ($H_2O/D_2O$ = 9:1, v/v) containing 0.002% $NaN_3$ and 0.01 mM EDTA, pH 4.0. Sodium 3-trimethylsilyl [2, 2, 3, 3-$2H_4$] propionate was added at a final concentration of 200 μM as an internal chemical shift reference. All NMR spectra were recorded from a 500-MHz Bruker DRX-500 spectrometer at 295 K.

### 2.4.3 Electrophysiological experiments

Rat DRG neurons were acutely dissected and maintained in as short-term cultures as described by Gu et al. (1998) and Li et al. (2003). The patch-clamp experiments were performed at 25°C under the whole cell configuration. Patch pipettes (2–3 μm diameter) were pulled from borosilicate glass capillary tube by using a two-step vertical puller (PC-10, Narishige, Olympus) and heat-polished with a microforge (MF-900, Narishige). Patch pipettes with resistances of 2.0–3.0 megaohms were used. The pipette solution contained 105 mM CsF, 35 mM NaCl, 10 mM HEPES with the pH adjusted to 7.4 with 1 M CsOH. The external bathing solution contained 150 mM NaCl, 2 mM KCl, 5 mM D-glucose, 1 mM $MgCl_2$, 1.5 mM $CaCl_2$, 10 mM HEPES with the pH adjusted to 7.40 with 1 M NaOH.

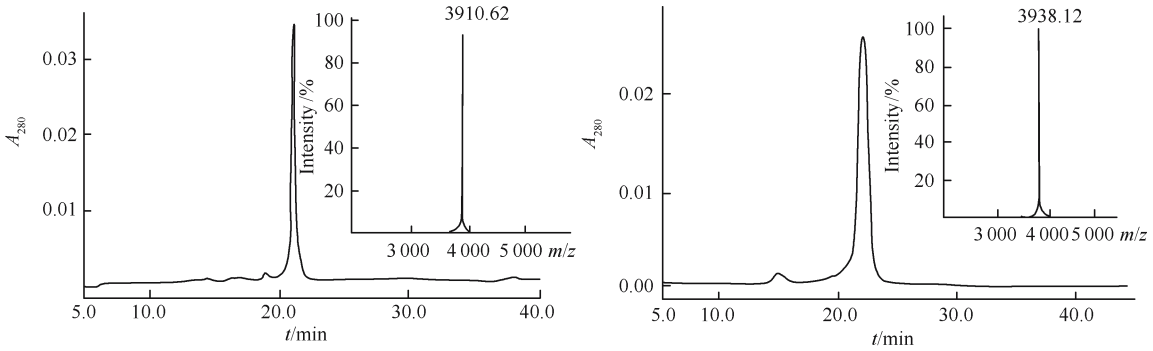


(a) and (b) illustrate the RP-HPLC and MALDI-TOF MS profile of R26A-HNTX-IV and K27A-HNTX-IV, respectively; The crude synthetic products of R26A-HNTX-IV and K27A-HNTX-IV were loaded to a Vydac C18 column (4.6 mm × 250 mm) pre-equilibrated with 0.1% aqueous TFA; elution was performed with a linear gradient 10%–45% acetonitrile over 45 min at a flow rate 1 mL/min at 40°C

**Fig. 1** Identification of crude synthetic HWNX-IV mutants

## 3 Results and discussion

### 3.1 Synthesis and purification of HNTX-IV mutants

Unambiguous peaks were detected for the crude synthetic products of R26A-HNTX-IV and K27A-HNTX-IV mutants in their RP-HPLC spectra, with corresponding molecular weights of 3 909.62 Da and 3 937.12 Da as determined by MALDI-TOF, which were identical to the theoretically calculated values (Fig. 1). These results suggested the successful synthesis of both R26A-HNTX-IV and K27A-HNTX-IV mutants.

### 3.2 Oxidation refolding of HNTX-IV mutants

Oxidation refolding of R26A-HNTX-IV and K27A-HNTX-IV were carried out in 0.1 M Tris-HCl, 0.1 M NaCl, pH 7.8, containing 5 mM GSH, 0.5 mM GSSG for 24 h. The successfully refolded R26A-HNTX-IV and K27A-HNTX-IV mutants

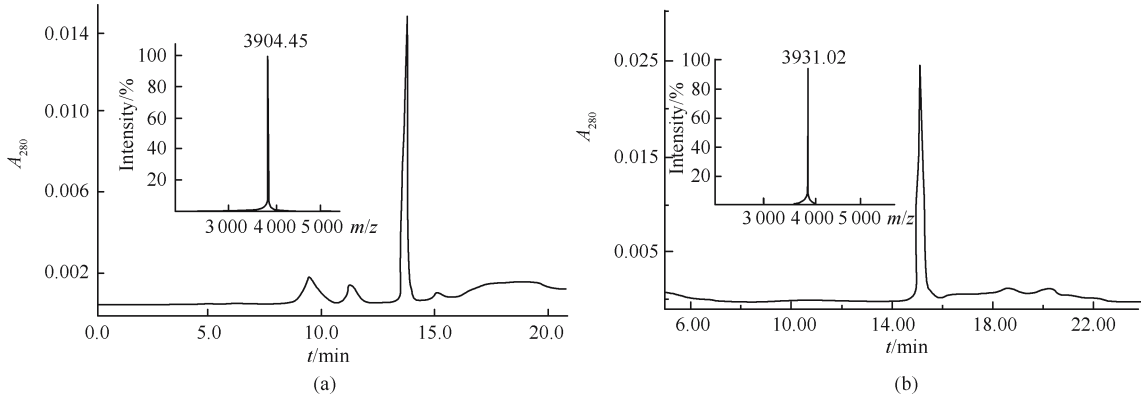


(a) and (b) illustrate the RP-HPLC and MALDI-TOF MS profile of refolded R26A-HNTX-IV and K27A-HNTX-IV, respectively. The refolded R26A-HNTX-IV and K27A-HNTX-IV mutants were applied to a Vydac C18 column (4.6 mm × 250 mm) previously equilibrated with 0.1% aqueous TFA. Elution was performed with a linear gradient 15%−45% acetonitrile over 50 min at a flow rate 1 mL/min at 40°C.

**Fig. 2** Identification of refolded HNTX-IV mutants

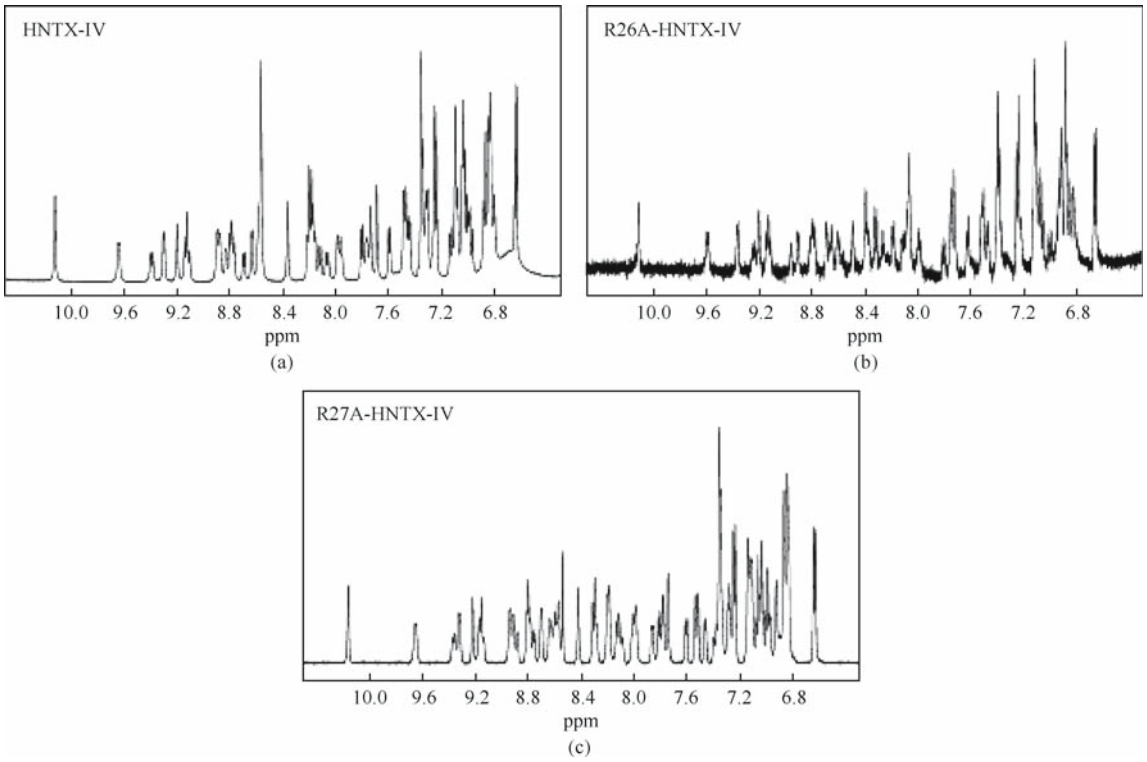


(a), (b) and (c) showe the amide proton region of one-dimensional $^1$H NMR spectra recorded for native HNTX-IV, R26A-HNTX-IV and K27A-HNTX-IV, respectively. Most of the resonance peaks remain identical.

**Fig. 3** One-dimensional $^1$H NMR spectra of native HNTX-IV and HNTX-IV mutants

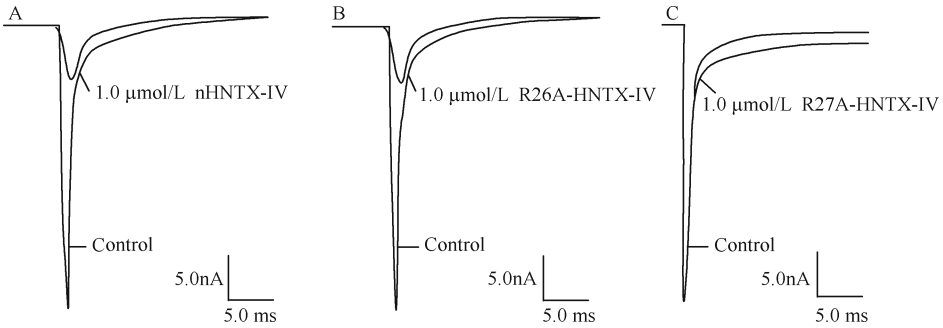


(A), (B) and (C) show the differentiated inhibitory effects of R26A-HNTX-IV and K27A-HNTX-IV on TTX-S sodium currents recorded from rat DRG neurons. Inhibition at potency similar to that of native HNTX-IV was observed in R26A-HNTX-IV, whereas nearly a complete loss in activity for K27A-HNTX-IV.

**Fig. 4** Effects of native HNTX-IV and HNTX-IV mutants on TTX-S sodium current

were fractioned by RP-HPLC and their individual average molecular masses were determined to be 3 904.35 Da and 3 930.02 Da, respectively, using MALDI-TOF. The detected molecular mass deviated 6 Da from the theoretical molecular mass for both R26A-HNTX-IV and K27A-HNTX-IV mutants, which indicated the formation of three pairs of disulfide bonds in them (Fig. 2).

### 3.3 Structural alteration in HNTX-IV mutants

One- and two-dimensional $^1$H NMR spectroscopies were widely used to analyze the structures of the synthetic analogues, to determine the extent of isomer purity and to assess the conformational integrity. In the amide proton region of one-dimensional $^1$H-NMR spectra recorded for native HNTX-IV, R26A-HNTX-IV and K27A-HNTX-IV, shifts of some resonance peaks were observed; however, the overall distribution looked similar, which suggested that no significant changes in the overall folding were introduced by mutations at Arg26 and Lys27 (Fig. 3). Furthermore, the secondary structure analysis of R26A-HNTX-IV and K27A-HNTX-IV by 2D $^1$H-NMR also indicated that they differed little from native HNTX-IV in their tertiary structures (data not shown).

### 3.4 Bioactivity assay of HNTX-IV mutants

The relevant changes in bioactivity for the refolded R26A-HNTX-IV and K27A-HNTX-IV were examined by patch-clamp experiments on DRG neurons. In comparison with 78% inhibition of sodium current by 1 μmoL/L native HNTX-XI, 76% inhibition and 26% inhibition by R26A-HNTX-IV and K27A-HNTX-IV were detected at the same dose, respectively (Fig. 4). The individual $IC_{50}$ value of R26A-HNTX-IV and K27A-HNTX-IV were calculated as 99.6 nmol/L and 3.22 μmol/L, respectively, whereas it was 34.0 nmol/L for native HNTX-IV (Fig. 5). As the inhibitory effect of K27A-HNTX-IV was about two grades lower than that of R26A-HNTX-IV, Lys27 appeared to be a residue of

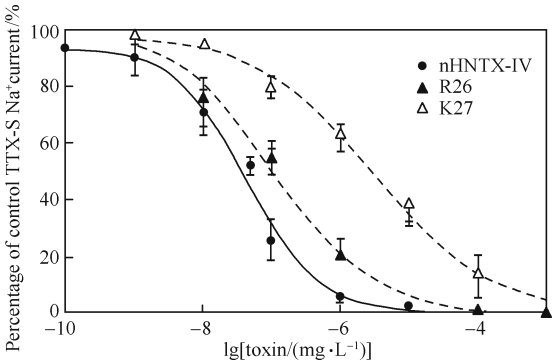


The dose-dependency curve of R26A-HNTX-IV's inhibition against TTX-S sodium currents shifted slightly from that of native HNTX-IV whereas it was significantly deviated for that of K27A-HNTX-IV.

**Fig. 5** Dose-dependent inhibition of native HNTX-IV and HNTX-IV mutants

critical role for HWNX-IV's interaction with the sodium channel.

As it is general for ICK toxins to use positively charged residues to interact with negatively charged residues in various types of ion channels, which is of crucial importance for target recognition of these toxins, the current work achieved a successful clarification of the differentiated roles of Arg26 and Lys27 in HWNX-IV in the inhibition of TTX-S sodium channels. However, in HNTX-IV there might be some other active sites awaiting characterization. Further work on mutation at these potential active sites is still ongoing, which would bring insights into the gating behavior of TTX-S sodium channels.

## References

Dai J, Liang S P (2003). Purification and characterization of huwentoxin-VII and huwentoxin-VIII, two novel insecticidal neurotoxins from the Chinese bird spider *Ornithoctorus huwena*. Chin. J Biochem. Mol. Biol., 19(4): 488−492 (in Chinese)

Gu Q H, Li ZW, Fan Y Z (1998). Modulation of bradykinin on ATP-activated currents in isolated rat DRG neurons. Acta Physiol. Sin., 50(1): 37−42 (in Chinese)

Li D L, Xiao Y C, Hu W J, Xie J Y, Bosmans F, Tytgat J, Liang, S P (2003). Function and solution structure of hainantoxin-I, a novel insect sodium channel inhibitor from the Chinese bird spider *Ornithoctorus hainana*. FEBS Lett., 555(3): 616−622

Liang S P, Peng X J, Huang R H, Chen P (1999). Biochemical identification of *Ornithoctorus hainana sp. nov*. from South China (Araneae, Theraphosidae). Life Sci. Res., 3(4): 299−303 (in Chinese)

Liang S P, Xia Z X, Xie J Y (1997). Solid-phase chemical synthesis and the bioactivity identification of Huwentoxin-I. Sci. China Ser. C, 27(5): 449−457 (in Chinese)

Liu Z H, Chen P, Liang S P (2002). Synthesis and oxidative refolding of Hainantoxin-IV. Acta Biochim. Biophys. Sin., 34(4): 516−519 (in Chinese)

Liu Z H, Dai J, Chen Z R, Hu W J, Xiao Y C, Liang S P (2003). Isolation and characterization of hainantoxin-IV, a novel antagonist tetrodotoxin-sensitive sodium channels form the Chinese bird spider *Ornithoctorus hainana*. Cell Mole Life Sci., 60: 972−978

Wang X C, Liang S P, Luo Z M (2000). Solid-phase synthesis and bioactivity analysis of A1Y-HWTX-I:a mutant of huwentoxin-I. Chin. J. Biochem. Mol. Biol., 16(3): 357−362 (in Chinese)

Xiao Y C, Liang S P (2003). Inhibition of sodium channels in rat dorsal root ganglion neurons by hainantoxin-IV, a novel spider toxin. Acta Biochim. Biophys. Sin., 35(1): 82−85 (in Chinese)